CRYSTAL GROWTH & DESIGN

pubs.acs.org/crystal

Article

Valence Band Modulation Using Cationic Filled p Orbitals toward p-Type Conduction

Hiroshi Mizoguchi,* Satoru Matsuishi, Hiroyo Segawa, Noriko Saito, and Hideo Hosono*

Cite This: *Cryst. Growth Des.* 2025, 25, 1892−1896

Read Online

ACCESS | Metrics & More | Article Recommendations | Supporting Information

ABSTRACT: p-Type conduction is difficult in wide-gap compound semiconductors, such as transparent oxides. Anionic p orbitals primarily constituting the valence band maximum (VBM) are localized owing to their highly electronegative nature, which gives rise to a large ionization potential (Ip), leading to a difficulty in hole doping into the VBM. Here, we report a new approach to VBM modulation through the covalent interaction with filled cationic p orbitals. LaN is taken as an example. Pushing the anionic valence band (VB) to VBM by σ interaction in N−La chains between the N 2p VB and the filled La p orbitals decreases Ip and enhances the dispersion of VBM, leading to a direct-type band gap. Cationic p states (La $5p^6$) located energetically near the VB and linear coordination of La−N chains present in rock-salt-type crystal structures are keys to making the N p−La p covalent interaction strong.

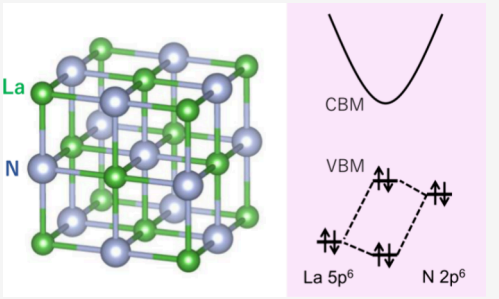

INTRODUCTION

Transparent oxide semiconductors (TOSs) are attracting much attention as thin film transistor channels for driving flat panel displays and transistors for high-power applications with high mobility, good durability, large band gap, and low production cost. The representative examples for applications are amorphous indium gallium zinc oxide for the backplane to drive flat panel displays and Ga_2O_3 single crystals for power transistors.[1−3] However, the conduction type of TOSs is practically restricted to the n-type, which is a major obstacle to extending the applications of TOSs. This difficulty primarily comes from the intrinsic nature of large band gap ionic compounds; i.e., the nature of the valence band maximum (VBM) is to work as the hole pathway, whereas the conduction band minimum (CBM) serves as the electron pathway. Oxygen 2p orbitals primarily constituting the VBM are localized owing to the high electron negativity of oxygen and the absence of other orbitals of nearby cations shown schematically in Figure 1a, which are rather different from the spatially extended vacant cationic orbitals constituting the CBM. Consequently, the ionization potential ((Ip), E(VBM) − E(Vac)) is large, whereas the electron affinity (E(CBM) − E(Vac)) is small. Such a large Ip makes it difficult to dope positive holes into VBM, and a large effective mass of holes at VBM suppresses the mobility of the doped holes.[4a,b] These are the general reasons why p-type conduction is difficult in wide-gap ionic compounds such as TOSs. Figure 1b−d summarizes the approach to p-type TOSs reported to date. The p orbitals have directional and ungerade symmetry, which makes them less likely to interact with the surrounding orbitals and form covalent bonds. In particular, 2p orbitals are considerably contracted among np orbitals (principal quantum number, n = 2−6). In the periodic table, orbitals with the smallest number of n are significantly contracted. To overcome this obstacle, in the electronic structure design of p-type TOSs, it is often aimed to increase the VB dispersion by giving them covalent bonding characteristics. For example, in SnO, the Sn^{2+} $5s^2$ orbital, called the cationic lone pair, is utilized. The Sn 5s state having stereochemical activity is located at about the same

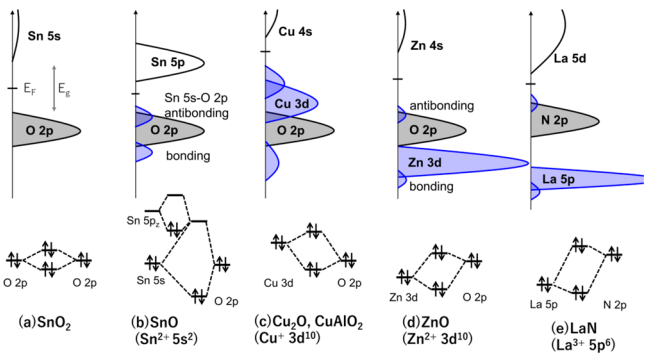

Figure 1. VB modulation by the addition of covalent interactions in TOSs. (a) Post-transition-metal oxides commonly have VB composed of oxygen 2p orbitals. (b−e) VB modulation through covalent interaction with filled cationic bands, which pushes up the VBM.

Received: January 6, 2025
Revised: February 24, 2025
Accepted: February 25, 2025
Published: March 4, 2025

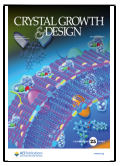

https://doi.org/10.1021/acs.cgd.5c00012
Cryst. Growth Des. 2025, 25, 1892−1896

energy level as that of the 2p O state, and the two interact strongly to give rise to VB dispersion.[5a,b] In Cu_2O or $CuAlO_2$, an increase in O 2p band dispersion is achieved by hybridizing shallow cationic d orbitals (Cu $3d^{10}$).[6] In ZnO, the VBM is modulated by filled Zn $3d^{10}$ states that locate at an energy level close to that of O 2p VB.[7] This is enhanced also by a short distance d_{Zn-O} in the tetrahedral coordination. Occupied S-states such as s^2 or d^{10} have zero orbital angular momentum. Such an orbital with an isotropic and gerade phase in cations has relatively easy interaction with the contracted anionic 2p orbitals as well. Here, we propose a novel approach to designing p-type TOSs by utilizing the filled p orbitals of cations. To embody this concept, we set the following two required conditions. (1) A crystal structure having metal cation (M)−anion (X) chains: The *M* p−*X* p σ interaction depends highly on the angle θ (Scheme 1) showing a maximum at θ =

Scheme 1. *M* p−*X* p Chain

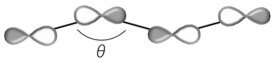

180°. (2) We select occupied cationic np^6 states having an energy level slightly deeper than that of oxygen 2p. The covalent interaction between these states pushes up the VB constituted by anion 2p, as shown in Figure 1e. This generates a rock-salt-type crystal structure, *MX* (Figure 2a), which meets

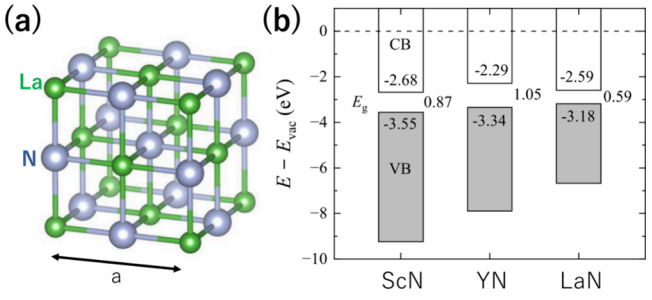

Figure 2. (a) Crystal structure of LaN (rock-salt-type, lattice constant *a* = 5.30 Å). (b) Calculated positions of VBM and CBM for *MN* (*M* = Sc, Y, or La).

both requirements. In the structure, MX_6 octahedra share the edges with each other to form an *M*−*X* chain running along the *a*, *b*, or *c* direction. Here, we focus on cubic LaN on the basis of its characteristic VB structure elucidated through DFT calculations and experiments.

EXPERIMENTAL SECTION

DFT periodic calculations for the survey of compounds with the rock-salt-type crystal structure (*MN* with *M* = Sc, Y, La, or Ce and *MO* with *M* = Ca, Sr, or Ba) were performed using the generalized gradient approximation and spin orbit coupling as implemented in VASP.[8a,b] We used the HSE06 hybrid functional[9a,b] for structural optimization, electronic bands, and optical absorption spectrum calculations. No Hubbard term was taken into account for the 4f states of La or Ce. All of the calculations were performed with the primitive cell obtaining one chemical formula, *MO* or *MN*. A kinetic energy cutoff of 520 eV with a 6 × 6 × 6 Γ-centered k-point mesh and a cutoff of 400 eV with a k-path of 2.5 Å point density were respectively used for structural optimization and electronic band calculation. The irreducible representations of plane wave-based spinor wave functions at high symmetry points in the double space group[10] were determined using the Irvsp code.[11] The Wigner−Seitz radius (R_{wigs}) for site projections for all atoms was selected to satisfy the equation $V = N \cdot 4/3\ \pi R_{wigs}^3$ where *V* is the volume of the unit cell and *N* is the total number of atoms in the unit cell. To assist in understanding the nomenclature of the reciprocal space, the Brillouin zone of the cubic F-lattice is shown in Figure S1 in the Supporting Information.

The band alignment of *MN* relative to the vacuum level was obtained using the electrostatic potential calculated with the (100) slab model without surface relaxation, consisting of the nine *MN* atomic layers (thickness ∼20 Å) and a vacuum space of ∼25 Å.

A polycrystalline sample of LaN was synthesized by solid-state reactions at high temperatures. The starting material used was the LaN (99.9%) powder purchased from AlfaAesar. The nitride was heated to 1023 K for 10 h under ammonia. The resulting brownish black powder was air-sensitive. The crystal structures of the synthesized materials were examined by powder X-ray diffraction (RIGAKU MINIFLEXII) using Cu K_α radiation. The X-ray data were collected in the range 2θ = 5−90° at 0.02° intervals at room temperature. The obtained powder XRD pattern indicates that LaN has a cubic rock-salt-type crystal structure, as shown in Figure S2. UV−vis-NIR diffuse reflectance data were collected in the spectral range of 240−2600 nm with a Shimadzu SolidSpec-3700 spectrometer using MgO as a reference. The Kubelka−Munk function was used to transform the data into absorbance.

RESULTS AND DISCUSSION

First, Figure S3 shows the calculated band structures of the alkaline earth oxide *MO* (*M* = Ca, Sr, or Ba). The binding energy (*E* = 0) is referenced to the VBM. The O $2p_y$ orbital is highlighted in red with a fat-band representation. All three compounds have large band gaps, and BaO has the smallest band gap (E_g = 3.0 eV) among the three. Whereas these compounds with a highly ionic bonding nature often adopt the rock-salt-type crystal structure, the band dispersion in the k space is seen for CBM and VBM. This result means that the participation of the covalent bonding nature is not negligibly small even in these ionic compounds. The CBM is located at the X point in these oxides. The widespread band near CBM originates from *M* *n*d orbitals, and the alkali earth ion *M* behaves like an early transition metal ion. On the other hand, the VB is mainly composed of O 2p, and the bandwidth decreased in the order of CaO, SrO, and BaO. CaO or SrO with VBM at the Γ point has an indirect-type band gap. Interestingly, the O $2p_y$ band in BaO is pushed up at the X point to form VBM, resulting in the direct-type band gap. The O 2p band splits into two at the X point, (0 1 0), owing to the symmetry. One is O $2p_y$; the other is degenerated O $2p_x$ $2p_z$. Although the O $2p_y$ band locates at −2 eV from the VBM in CaO, it shifts to the VBM (*E* = 0 eV) in BaO. Next, Figure S4 shows calculated band structures of *MN* (*M* = Sc, Y, La, or Ce) nitrides. *MN* (*M* = Sc, Y, or La) is a semiconductor, and LaN has the smallest band gap (E_g = 0.59 eV) among the three. Interestingly, the calculated band gap of LaN is much smaller than the experimental one of La_2O_3 (E_g = 5.2 eV). The calculated indirect-type band gap of ScN (0.87 eV) is consistent with the experimental value (0.92 eV).[12] The large dispersion of CBMs in these nitrides is very similar to that in *MO*s, and the M^{3+} ion also behaves similarly to a d-block ion. Unoccupied La 4f orbitals locate at ∼+7 eV to form narrow bands. VB in *MN*s is mainly composed of the N 2p band, and the bandwidth decreases from that of ScN to that of LaN through YN. ScN or YN with VBM at the Γ point has the indirect-type band gap. Interestingly, in LaN, the N $2p_y$ band is pushed up at the X point to form VBM, resulting in the direct-type band gap, as seen in BaO. The behavior of N 2p bands at

https://doi.org/10.1021/acs.cgd.5c00012
Cryst. Growth Des. 2025, 25, 1892−1896

the X point is the same as that of O 2p in the *M*O series. Although CeN has a metallic nature because of the unique electronic configuration of the Ce^{3+} ion ($5d^14f^0$),[13] the behavior of N $2p_y$ band in CeN is similar to that of LaN. Figure 2b shows the calculated VBM and CBM positions for *M*N (*M* = Sc, Y, or La). The position of the VBM in LaN is highly pushed up among the three, indicating the decrease in Ip. The results of the survey of *M*O and *M*N series exhibit the following two tendencies for VB: With the principal quantum number *n*, (1) the VB width decreases because of the increase in ionic bonding characteristic of $M^{n+}-X^{n-}$ interaction, and (2) the anion p_y band is largely pushed up at the X point to form VBM, resulting in the direct-type band gap.

To reveal the implications of the bonding interaction, we examined the band structure of LaN (Figure 2a) in greater depth. Figure 3a shows the details of the band structure again.

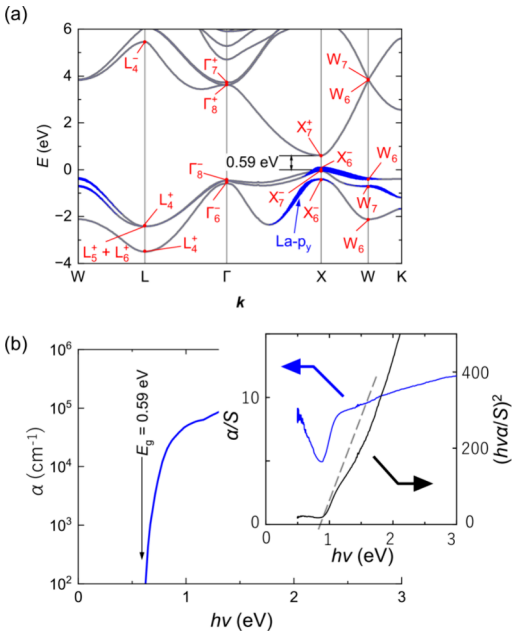

Figure 3. (a) Band electronic structure of LaN. The contribution from the La p_y orbital is highlighted with a fat-band representation in blue. (b) Calculated absorption spectrum near the band gap for LaN. Inset: diffuse reflectance spectra.

The La $5p_y$ orbital is highlighted in blue with a fat-band representation. Most of the features of the calculated band structure agree well with the previous reports.[14a−f] A semiconductor with the direct-type band gap at the k position except for the Γ point is very rare. Figure 4a shows schematics of orbital interactions of LaN at the CBM and VBM at the X point. The CBM, which does not contain the contribution of anion orbitals, is deepened by the direct La t_{2g}−La t_{2g} covalent interaction. In the crystal structure, LaN_6 octahedra share edges with each other, resulting in the shorter distance d_{La-La}. A smaller lattice arising from a shorter *M*−*M* separation enhances the d−d bonding as well, as seen in CeN with ∼5.0 Å (Figure S4d). On the other hand, the behavior of VB is more complicated. The band is mainly composed of three N 2p orbitals. At the X point, the N $2p_y$ band is pushed up to form VBM by its covalent interaction with La $5p_y$ (blue fat-band) in the La−N chain, as shown in Figure 4a. This VB modulation is similar to that in ZnO caused by the O 2p−Zn 3d covalent interaction (Figure 1d). From Figure S4c, the 5p bands in LaN

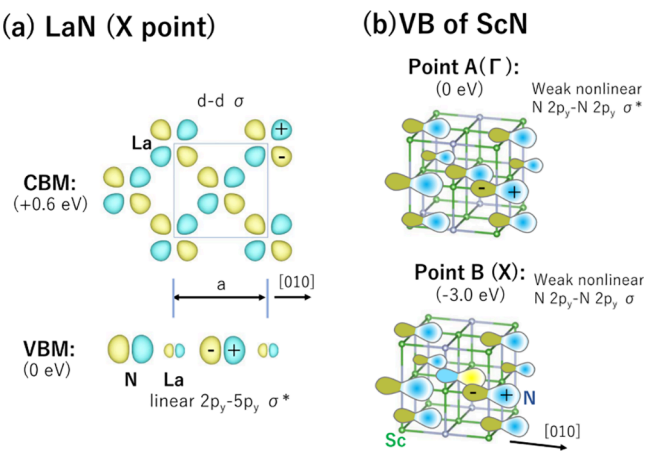

Figure 4. (a) Orbital interactions at the CBM or VBM in LaN. (b) Orbital interactions at VB in ScN, shown in Figure S4a. One of the three degenerated N 2p bands is shown for point A.

locate at a relatively shallow position ($E \sim -15$ eV), making the interaction with the VB composed of N 2p possible. The semicore-like 5p bands split into $p_{3/2}$ and $p_{1/2}$ owing to the spin orbit interaction (SOI). On the other hand, 2p bands of light N do not split owing to the small SOI, which is proportional to Z^4 (*Z*: atomic number). However, the 2p bands are split weakly by covalent interaction with the split La 5p. As shown in Figure S 4d, the modulation of the N $2p_y$ band in CeN is larger than that in LaN, reflecting a stronger SOI of Ce rather than La. The appearance of the direct-type band gap of LaN originates from the peculiar behavior of the N $2p_y$ band. Here, we compare the behavior of N $2p_y$ in LaN with that in ScN having indirect-type band gap to clarify the modulation into the N $2p_y$ band. Although the N $2p_y$ band at the X point is located at −3 eV in ScN (Figure S4a), it shifts considerably to VBM (E = 0 eV) in LaN. Sc 3p bands locate at −29 eV (not shown in Figure S4a), which is too deep to interact with VB. Instead, a direct N 2p−N 2p covalent interaction works in ScN with a smaller lattice (d_{N-N} = 3.14 Å in ScN). Figure 4b shows the orbital interaction of the A (Γ) point and B (X) point in ScN, shown in Figure S4a. Weak N $2p_y$−N $2p_y$ σ^* antibonding and weak σ bonding work at the Γ and X points, respectively, which are not N−N linear chain. That is why the VB width is dominated by the direct N 2p−N 2p interaction (d_{N-N} = 3.14 Å) in ScN. On the other hand, the N−N interaction seen in ScN does not work in LaN with a larger lattice (d_{N-N} = 3.75 Å). Instead, semicore-like La 5p bands modulate VB to form a direct-type band gap. The irreducible representations (irreps) of the VBM and CBM states at the X point are determined to be X_6^- and X_7^+, respectively. The direct product of X_6^- and the irrep X_4^- of the electric dipole operators with the E_u characteristic (x, y) is X_7^+,[15] indicating that the transition between VBM and CBM is allowed. Figure 3b shows the calculated optical absorption of LaN near the band gap. It stands up steeply near 0.6 eV. The direct allowed band gap was experimentally estimated to be 0.90 eV from the $(h\nu\alpha/S)^2-h\nu$ plot (*S*: scattering coefficient) in the inset of Figure 3b, which is consistent with the calculated band gap. The observed weak absorption near 0.5 eV originates from free carriers in CB, probably induced by a N deficiency. This agrees with the formation enthalpy of N vacancy[14f] calculated by Deng and Kioupakis.

https://doi.org/10.1021/acs.cgd.5c00012
Cryst. Growth Des. 2025, 25, 1892−1896

The DFT calculation results for rock-salt-type compounds exhibit that the filled 5p bands of Ba, La, or Ce modulate VB. This finding forms the basis of the concept applicable to the fine-tuning of the VB design of TOSs. First, we discuss the reason these bands can modulate anionic VB. Can we extend this concept into np bands of other heavy metal cations? Figure 5 shows the reported energy level of semicore-like np

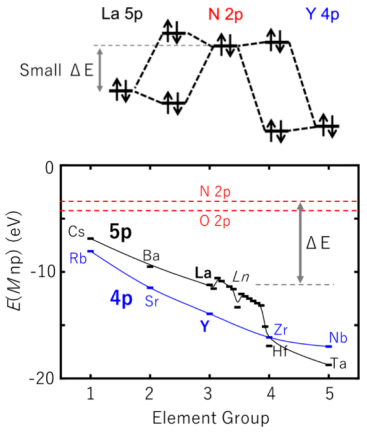

Figure 5. Calculated energy level of filled np state of heavy metal atoms.[16] The energy difference (ΔE) between the filled np state and anionic 2p VB is an important factor for the covalent interaction, which results in a large VB dispersion.

states of the fifth or sixth period atoms, which was calculated for the ground electronic configuration in the local density approximation.[16] Those of anionic 2p states are also shown to estimate the energetic overlap (ΔE) with the p states of heavy metal elements, which reflects the covalent interaction. The increased valence charge of an element makes the energy level deeper monotonically. For example, Br 4p bands often locate in the VB region near the Fermi energy in bromides. The 4p level deepens in the order of Br, Kr, Rb, Sr, and Y. The energy level of Y 4p states is too deep to interact with anionic 2p VB in the *M*N nitride. Thus, the cations residing in the left-side region of the periodic table have shallow np states. In the sixth period shown by a black line, the effect of lanthanide contraction also occurs. Figure 5 suggests that the shallow filled np bands of Cs, Rb, Ba, La, Ce, or Pr (Th) can modulate VB.

The N 2p−La 5p interaction observed in LaN does not commonly appear in the electronic structures of inorganic solids. In fact, it gives rise to a unique direct-type band gap that appears at the X point owing to the ungerade characteristic of N 2p orbitals. Finally, we discuss an example of similar semiconductors that utilize the contribution of cationic p states. Perovskite (PV)-type halides including $CsSnI_3$ often have the direct-type band gap at the R point for cubic primitive lattices, and they have been anticipated to be used as optical absorbers for solar cells.[17] A cubic PV-type structure is composed of a three-dimensional framework of corner-sharing SnI_6 octahedra, with the Cs^+ ions filling the cuboctahedral cavities. The I ions are linearly coordinated by two Sn atoms to form a chain, as seen in LaN. The top of VB is dominated by the contribution of I 5p hybridized by Sn 5s. CBM is dominated by the contribution of Sn 5p hybridized weakly by I 5s, as shown in Figure S5.[17,18] The top of the CB is composed of the Sn 5p−I 5p σ^* interaction in the Sn−I chain, which is very similar to the VBM of LaN. Thus, the unique positions of band edges in the k space are derived from the ungerade symmetry of the p orbitals. The PV halide layer sandwiched by electron and hole transport layers has been investigated as optical absorbers for solar cells, where photoexcited carriers are separated without recombination.[19] The high mobility of excited electrons originating from the widespread CB renders electron transport into n-type electrodes possible.

CONCLUSIONS

Anionic p orbitals constituting the VB often do not contribute to covalent bonding in solid compounds because of their directional shape and ungerade symmetry. However, the VBM modulation of LaN can be achieved through covalent interaction with filled cationic p bands. A VB structure can be designed by the careful tuning of the coordination structure, energy level, orbital radius of cationic p states, and SOI. In general, p-type doping into compound semiconductors becomes easier as the Ip decreases. Pushing the VB to VBM by the σ interaction between the anionic np orbitals constituting the upper VB and cation's filled p orbitals decreases Ip and enhances the dispersion of VBM, leading to the reduction in effective hole mass. Thus, this approach will be a novel way to design p-type semiconductors.

ASSOCIATED CONTENT

Supporting Information

The Supporting Information is available free of charge at https://pubs.acs.org/doi/10.1021/acs.cgd.5c00012.

Powder XRD pattern for LaN, the Brillouin zone, electronic structure calculations for *M*O (*M* = Ca, Sr, or Ba) and *M*N (*M* = Sc, Y, La, or Ce), and schematic density of states for $CsSnI_3$ (PDF)

AUTHOR INFORMATION

Corresponding Authors

Hiroshi Mizoguchi − *Research Center for Materials Nanoarchitectonics (MANA), National Institute for Materials Science (NIMS) Tsukuba, Ibaraki 305-0044, Japan;* orcid.org/0000-0002-0992-7449; Email: mizoguchi.hiroshi@nims.go.jp

Hideo Hosono − *Research Center for Materials Nanoarchitectonics (MANA), National Institute for Materials Science (NIMS) Tsukuba, Ibaraki 305-0044, Japan; MDX Research Center for Element Strategy, International Research Frontiers Initiative, Institute of Science Tokyo 4259 Nagatsuta, Yokohama 226-8503, Japan;* orcid.org/0000-0001-9260-6728; Email: hosono@mces.titech.ac.jp

Authors

Satoru Matsuishi − *Research Center for Materials Nanoarchitectonics (MANA), National Institute for Materials Science (NIMS) Tsukuba, Ibaraki 305-0044, Japan*

Hiroyo Segawa − *Research Center for Electronic and Optical Materials, National Institute for Materials Science (NIMS) Tsukuba, Ibaraki 305-0044, Japan*

Noriko Saito − *Research Center for Electronic and Optical Materials, National Institute for Materials Science (NIMS) Tsukuba, Ibaraki 305-0044, Japan;* orcid.org/0000-0002-8104-0172

Complete contact information is available at:

https://doi.org/10.1021/acs.cgd.5c00012
Cryst. Growth Des. 2025, 25, 1892−1896

https://pubs.acs.org/10.1021/acs.cgd.5c00012

Notes

The authors declare no competing financial interest.

■ ACKNOWLEDGMENTS

The calculations in this study were performed on the Numerical Materials Simulator at NIMS. This work was supported by a Grant-in-Aid for Scientific Research (23K23440) from the Japan Society for the Promotion of Science (JSPS). A part of this work was supported by the "Advanced Research Infrastructure for Materials and Nanotechnology in Japan (ARIM)" of the Ministry of Education, Culture, Sports, Science, and Technology (MEXT). Proposal JPMXP123NM5382.

■ REFERENCES

(1) Nomura, K.; Ohta, H.; Takagi, A.; Kamiya, T.; Hirano, M.; Hosono, H. Room-temperature fabrication of transparent flexible thin-film transistors using amourphous oxide semiconductors. *Nature* **2004**, *432*, 488−492.

(2) Hosono, H. Exploring Electro-active Functionality of Transparent Oxide Materials. *Jpn. J. Appl. Phys.* **2013**, *52* (9R), No. 090001.

(3) Oba, F.; Kumagai, Y. Design and exploration of semiconductors from first principles: A review of recent advances. *Appl. Phys. Express* **2018**, *11*, No. 060101.

(4) (a) Robertson, J.; Zhang, Z. Doping limits in p-type oxide semiconductors. *MRS Bull.* **2021**, *46* (11), 1037−1043. (b) Mizoguchi, H.; Woodward, P. M. Electronic Structure Studies of Main Group Oxides Possessing Edge-Sharing Octahedra: Implications for the Design of Transparent Conducting Oxides. *Chem. Mater.* **2004**, *16*, 5233−5248.

(5) (a) Ogo, Y.; Hiramatsu, H.; Nomura, K.; Yanagi, H.; Kamiya, T.; Hirano, M.; Hosono, H. p-channel thin-film transistor using p-type oxide semiconductor, SnO. *Appl. Phys. Lett.* **2008**, *93*, No. 032113. (b) Walsh, A.; Payne, D. J.; Egdell, R. G.; Watson, G. W. Stereochemistry of post-transition metal oxides: revision of the classical lone pair model. *Chem. Soc. Rev.* **2011**, *40* (9), 4455−63.

(6) Kawazoe, H.; Yasukawa, M.; Hyodo, H.; Kurita, M.; Yanagi, H.; Hosono, H. P-type electrical conduction in transparent thin films of $CuAlO_2$. *Nature* **1997**, *389*, 939−942.

(7) Wei, S.; Zunger, A. Role of metal d states in II-VI semiconductors. *Phys. Rev. B Condens Matter* **1988**, *37* (15), 8958−8981.

(8) (a) Kresse, G.; Furthmuller, J. Efficient iterative schemes for ab initio total-energy calculations using a plane-wave basis set. *Phys. Rev. B* **1996**, *54*, 11169−11186. (b) Kresse, G.; Joubert, D. From ultrasoft pseudopotentials to the projector augmented-wave method. *Phys. Rev. B* **1991**, *59* (3), 1758−1775.

(9) (a) Heyd, J.; Scuseria, G. E.; Emzerhof, M. Hybrid functionals based on a screened Coulomb potential. *J. Chem. Phys.* **2003**, *118* (18), 8207−8215. (b) Krukau, A. V.; Vydrov, O. A.; Izmaylov, A. F.; Scuseria, G. E. Influence of the exchange screening parameter on the performance of screened hybrid functionals. *J. Chem. Phys.* **2006**, *125* (22), No. 224106.

(10) Elcoro, L.; Bradlyn, B.; Wang, Z.; Vergniory, M. G.; Cano, J.; Felser, C.; Bernevig, B. A.; Orobengoa, D.; de la Flor, G.; Aroyo, M. I. Double crystallographic groups and their representations on the Bilbao Crystallographic Server. *J. Appl. Crystallogr.* **2017**, *50* (5), 1457−1477.

(11) Gao, J.; Wu, Q.; Persson, C.; Wang, Z. Irvsp: To obtain irreducible representations of electronic states in the VASP. *Comput. Phys. Commun* **2021**, *261*, No. 107760.

(12) Deng, R.; Ozsdolay, B. D.; Zheng, P. Y.; Khare, S. V.; Gall, D. Optical and transport measurement and first-principles determination of the ScN band gap. *Phys. Rev. B* **2015**, *91* (4), No. 045104.

(13) Landrum, G. A.; Dronskowski, R.; Niewa, R.; DiSalvo, F. J. Electronic Structure and Bonding in Cerium (Nitride) Compounds: Trivalent versus Tetravalent Cerium. *Chem. Eur. J.* **1999**, *5* (2), 515−522.

(14) (a) Hasegawa, A. Electronic structure of La monopnictides. *J. Phys. C: Solid State Phys.* **1980**, *13*, 6147−6156. (b) Stampfl, C.; Mannstadt, W.; Asahi, R.; Freeman, A. J. Electronic structure and physical properties of early transition metal mononitrides: Density-functional theory LDA, GGA, and screened-exchange LDA FLAPW calculations. *PhysRevB* **2001**, *63* (15), No. 155106. (c) Larson, P.; Lambrecht, W. R. L.; Chantis, A.; van Schilfgaarde, M. Electronic structure of rare-earth nitrides using the LSDA + *U* approach: Importance of allowing 4*f* orbitals to break the cubic crystal symmetry. *Phys. Rev. B* **2007**, *75* (4), No. 045114. (d) Zhao, E.; Wu, Z. Electronic and mechanical properties of 5d transition metal mononitrides via first principles. *J. Solid State Chem.* **2008**, *181* (10), 2814−2827. (e) Winiarski, M. J.; Kowalska, D. A Band gap bowings of ternary REN (RE= Sc, Y, La, and Lu) alloys. *J. Alloys. Compd.* **2020**, *824*, No. 153961. (f) Deng, Z.; Kioupakis, E. Semiconducting character of LaN: Magnitude of the bandgap and origin of the electrical conductivity. *AIP Adv.* **2021**, *11* (6), No. 065312.

(15) Gupta, M.; Jana, S.; Nanda, B. R. K. Electronic Structure and Optoelectronic Properties of Halide Double Perovskites: Fundamental Insights and Design of a Theoretical Workflow. *Chem. Mater.* **2024**, *36* (1), 132−145.

(16) Kotochigova, S.; Levine, Z. H.; Shirley, E. L.; Stiles, M. D.; Clark, C. W. Local-density-functional calculations of the energy of atoms. *Phys. Rev. A* **1997**, *55*, 191−199.

(17) Goesten, M. G.; Hoffmann, R. Mirrors of Bonding in Metal Halide Perovskites. *J. Am. Chem. Soc.* **2018**, *140* (40), 12996−13010.

(18) Seo, D.; Gupta, N.; Whangbo, M.; Hillebrecht, H.; Thiele, G. Pressure-Induced Changes in the Structure and Band Gap of $CsGeX_3$ (x = Cl, Br) Studied by Electronic Band Structure Calculations. *Inorg. Chem.* **1998**, *37*, 407−410.

(19) Snaith, H. J. Perovskites: The Emergence of a New Era for Low-Cost, High-Efficiency Solar Cells. *J. Phys. Chem. Lett.* **2013**, *4* (21), 3623−3630.